Applied Acoustics 191 (2022) 108662

Contents lists available at ScienceDirect

Applied Acoustics

journal homepage: www.elsevier.com/locate/apacoust

Benchmarking of finite-difference time-domain method and fast multipole boundary element method for room acoustics

Yue Li [a,d,*,1], Julie Meyer [b,1], Tapio Lokki [c], Jacques Cuenca [a], Onur Atak [a], Wim Desmet [d,e]

[a] Siemens Digital Industries Software, Interleuvenlaan 68, B-3001 Leuven, Belgium
[b] Department of Computer Science, Aalto University, Konemiehentie 29, FI-02150 Espoo, Finland
[c] Department of Signal Processing and Acoustics, Aalto University, Maarintie 8, FI-02150 Espoo, Finland
[d] Department of Mechanical Engineering, KU Leuven, Celestijnenlaan 300, B-3001 Heverlee, Belgium
[e] DMMS Core Lab, Flanders Make, Belgium

ARTICLE INFO

Article history:
Received 14 September 2021
Received in revised form 13 December 2021
Accepted 27 January 2022

Keywords:
room acoustic simulation
uncertainty
finite-difference time-domain method
fast multipole boundary element method

ABSTRACT

Compared to geometrical acoustics, wave-based methods which solve the wave equation either in the time domain or in the frequency domain are known for their high accuracy. However, their systematic use as professional room acoustic simulation tools is less popular due to the modelling effort and computational time requirements, especially in the case of complex scenarios. This paper aims at providing guidelines for the use of two wave-based methods in complex room acoustics simulations, namely the finite-difference time-domain (FDTD) method and the fast multipole boundary element method (FMBEM). Numerical experiments are conducted to address the convergence issues of the two solvers, more specifically, the selection of the convergence tolerance of the iterative solver in FMBEM and the temporal sampling frequency in FDTD. To evaluate the capability of the solvers in simulating complex scenarios, five cases with increasing complexity of material input data are presented. The results show that both solvers give close predictions for various room acoustics parameters. In addition, an uncertainty sensitivity study is performed in a case where experimental data is available. Large deviations between measured and simulated reverberation time reveal that typical material data-sets poorly represent the behaviour of real materials in a room acoustics context. Lastly, the efficiency of the two solvers is discussed. With parallelization implemented, both solvers can simulate sizeable room acoustic problems with good accuracy within a reasonable time.

1. Introduction

Digitalization brings new opportunities and innovations to many industries. In the context of room acoustics, computer-aided modelling and simulations have enabled efficient acoustic design, analysis and auralization [1,2]. Over the years, geometrical acoustics (GA) has been widely used and became the dominant solution for large geometrical models and/or at high frequencies. Various techniques including the image source method [3,4], ray and beam tracing techniques [5–7], have been developed and advanced. Such techniques usually simplify the sound waves as rays, and consider the energy and the propagation delay of each sound wave. The contribution perceived by the receiver is essentially the summation of either the energy component or the pressure component along the transfer paths. However, this "ray-like" propagation modelling may not be able to capture some of the wave phenomena. As a matter of fact, several state-of-the-art GA software were evaluated by recent round robin tests where large model errors and uncertainties were present due to the assumptions of GA and insufficient modeling of diffraction [8].

In the mid-low frequency range, especially when wave phenomena are prominent, wave-based methods are reported to be more accurate [9,10]. However, it is not obvious that they can give convincing results out of the box considering the complexities of the algorithms and the numerical uncertainties. In addition, there seems to be a lack of round robin tests for the wave-based methods in room acoustic modelling and simulations in the literature. This paper selects and evaluates two representative numerical methods: the fast multipole boundary element method (FMBEM) and the finite-difference time-domain (FDTD) method. The frequency domain BEM is known as a convenient numerical method for unbounded acoustic problems as its integral equation inherently

* Corresponding author.
E-mail address: li.yue@siemens.com (Y. Li).
[1] These authors contributed equally to this work.

https://doi.org/10.1016/j.apacoust.2022.108662
0003-682X/

satisfies the Sommerfeld radiation condition [11]. The fast multipole method (FMM) [12] enables BEM to handle large acoustic models at high frequencies, thus making it more efficient in solving large bounded problems such as room acoustics [13–15]. As a classical time-domain simulation method, FDTD has shown good capabilities in a wide range of acoustic applications including room acoustic simulations [1,16,17]. In practice, however, it is a non-trivial task to accurately simulate a complex scenario with complex geometry and multiple frequency-dependent materials. In order to evaluate the capability of the two solvers in simulating such complex scenarios, five cases in which the material input data is gradually complexified are presented.

To interpret and understand the simulated results, the uncertainties from the numerical simulations shall be clarified. In addition to the uncertainties from the model geometry [18] and material input data [7,10], the quantification of uncertainty specific to each numerical solver is essential as it indicates the reliability of the solution. Since the two wave-based solvers differ substantially, the numerical setups and conversions, e.g., for the acoustic source and boundary conditions, are addressed in order to avoid the misaligned input for the two solvers. The convergence issue which affects both accuracy and efficiency is critical for both solvers. Numerical experiments are conducted to discuss the selection of the convergence tolerance in FMBEM and the temporal sampling frequency in FDTD.

Last but not least, the limitations of wave-based solvers are generally attributed to their high computational cost, especially when the problem size gets large. Recent advances in high-performance computing (HPC) systems such as multi-core and many-core architectures [16,19,20] allow for efficient parallelization strategies and thus reduce the computational time significantly. In the acoustic scenarios presented here, it is shown that the algorithm enhancement, e.g., FMM for BEM, and the hardware accelerations from HPC strengthen the capabilities of the wave-based methods in simulating frequencies below the Schroeder frequency and well above.

The paper is organized as follows. Section 2 reviews the formulations derived in the FMBEM and FDTD solvers. The definitions and conversions of acoustic source and boundary conditions between the two solvers are also addressed. Section 3 gives an overview of the uncertainties in room acoustic simulations when using the two wave-based solvers. In Section 4, the selection of the convergence tolerance in FMBEM and the sampling frequency in FDTD are discussed via numerical experiments. Five scenarios with increased material input data complexity are presented in Section 5 in order to evaluate the capability of the solvers in simulating multiple frequency-dependent materials. The uncertainties of the material input data from two data-sets are quantified to better understand the discrepancies observed in the comparison between simulations and measurements. Section 5 also discusses the computational efficiency of the two solvers to demonstrate the potentials of the solvers in practical simulations.

2. Numerical methods

2.1. Mathematical formulation for acoustic problems

The linear wave equation is expressed in the 3D Cartesian coordinate system as follows

$$\frac{\partial^2 p}{\partial t^2} = c^2 \nabla^2 p, \tag{1}$$

where $\nabla^2 = \left(\frac{\partial^2}{\partial x^2} + \frac{\partial^2}{\partial y^2} + \frac{\partial^2}{\partial z^2}\right)$ is the Laplace operator, $p(x,y,z,t)$ is the acoustic pressure, and c is the speed of sound in the fluid.

When dealing with time-harmonic linear acoustic waves, i.e., continuous waves at constant angular frequency ω which yields a harmonic time dependence of $e^{-i\omega t}$, the governing differential equation can be written as the Helmholtz equation

$$\nabla^2 p + k^2 p = 0, \tag{2}$$

where $p(x,y,z,k)$ is the steady acoustic pressure and $k = \omega/c$ is the acoustic wavenumber at angular frequency ω.

2.1.1. Explicit FDTD formulation

To solve Eq. (1) for p using the explicit FDTD method, Eq. (1) is discretized in space and time and the second-order partial derivatives are substituted with finite differences, leading to, for the 3D standard rectilinear (SRL) scheme adopted here (Ref. [21], p.332),

$$\delta_t^2 p_{l,m,i}^n = \lambda^2 \left(\delta_x^2 + \delta_y^2 + \delta_z^2\right) p_{l,m,i}^n, \tag{3}$$

where $\lambda = cT/X$ is the Courant number with time step T and grid spacing X. $p_{l,m,i}^n \equiv p(x,y,z,t)|_{x=lX,y=mX,z=iX,t=nT}$ is the update variable, n denotes the time index and l, m, and i are the spatial indices in the x-, y-, and z-direction, respectively. $\delta_t^2, \delta_x^2, \delta_y^2, \delta_z^2$ are the second-order derivative centered finite-difference operators defined as

$$\delta_t^2 p_{l,m,i}^n \equiv p_{l,m,i}^{n+1} - 2p_{l,m,i}^n + p_{l,m,i}^{n-1}, \tag{4}$$

$$\delta_x^2 p_{l,m,i}^n \equiv p_{l+1,m,i}^n - 2p_{l,m,i}^n + p_{l-1,m,i}^n, \tag{5}$$

$$\delta_y^2 p_{l,m,i}^n \equiv p_{l,m+1,i}^n - 2p_{l,m,i}^n + p_{l,m-1,i}^n, \tag{6}$$

$$\delta_z^2 p_{l,m,i}^n \equiv p_{l,m,i+1}^n - 2p_{l,m,i}^n + p_{l,m,i-1}^n. \tag{7}$$

The update equation, expressing the future pressure values as a function of the present and past pressure values, can be found by substituting expressions 4-7 into Eq. (3), leading to

$$p_{l,m,i}^{n+1} = \lambda^2 \left(p_{l+1,m,i}^n + p_{l-1,m,i}^n + p_{l,m+1,i}^n + p_{l,m-1,i}^n + p_{l,m,i+1}^n + p_{l,m,i-1}^n\right) + 2(1 - 3\lambda^2) p_{l,m,i}^n - p_{l,m,i}^{n-1}. \tag{8}$$

Additionally, the FDTD simulations were run with the forward difference boundary meaning that the centered difference formulation of the partial derivative in the time domain and the forward difference formulation in the spatial domain are used. With such formulation, the boundary conditions can be expressed by

$$\frac{p_{l,m,i}^{n+1} - p_{l,m,i}^{n-1}}{2T} = -c\xi \frac{p_{l+1,m,i}^n - p_{l,m,i}^n}{X}, \tag{9}$$

$$\frac{p_{l,m,i}^{n+1} - p_{l,m,i}^{n-1}}{2T} = -c\xi \frac{p_{l,m+1,i}^n - p_{l,m,i}^n}{X}, \tag{10}$$

$$\frac{p_{l,m,i}^{n+1} - p_{l,m,i}^{n-1}}{2T} = -c\xi \frac{p_{l,m,i+1}^n - p_{l,m,i}^n}{X}, \tag{11}$$

where ξ is the specific acoustic impedance of the boundary ($\xi = \frac{1+R}{1-R}$). Finally, by deriving Eq. (8) for different node positions a general solution for the node update can be expressed by

$$p_{l,m,i}^{n+1} = \frac{1}{1+\lambda\beta}\left[\lambda^2 \left(p_{l+1,m,i}^n + p_{l-1,m,i}^n + p_{l,m+1,i}^n + p_{l,m-1,i}^n + p_{l,m,i+1}^n + p_{l,m,i-1}^n\right) + \left(2 - K\lambda^2\right) p_{l,m,i}^n + (\lambda\beta - 1) p_{l,m,i}^{n-1}\right], \tag{12}$$

where $\beta = \frac{(6-K)}{2\xi}$, and K equals 6 in free space, 5 at a wall, 4 at an edge, and 3 at a corner.

2.1.2. Indirect BEM and fast multipole acceleration

The frequency domain BEM relates the field variables in the continuum domain to the distribution of the associated boundary variables on the boundary surface of the domain. As such, it only requires the discretization of the boundaries of the target problem.

In an indirect boundary integral formulation [22], the boundary variables are the single-layer and double-layer potentials defined

as the difference of the normal derivative of the pressure and of the pressure across the boundary surface Γ, respectively. They can be written as

$$\sigma(\boldsymbol{y}) = \frac{\partial p(\boldsymbol{y}^+)}{\partial n_{y^+}} - \frac{\partial p(\boldsymbol{y}^-)}{\partial n_{y^-}},\ \boldsymbol{y} \in \Gamma, \tag{13}$$

$$\mu(\boldsymbol{y}) = p(\boldsymbol{y}^+) - p(\boldsymbol{y}^-),\ \boldsymbol{y} \in \Gamma, \tag{14}$$

where $\boldsymbol{y}$ denotes a source position vector on the boundary surface Γ and the superscripts + and − are associated with the same and opposite direction of the unit normal vector n_y to Γ, respectively. Using the single- and double-layer potentials, the acoustic pressure at the position vector $\boldsymbol{x}$ in the acoustic domain Ω is given by the indirect Kirchhoff-Helmholtz integral equation

$$p(\boldsymbol{x}) = \int_\Gamma \left[G(\boldsymbol{x},\boldsymbol{y})\sigma(\boldsymbol{y}) - \frac{\partial G(\boldsymbol{x},\boldsymbol{y})}{\partial n_y}\mu(\boldsymbol{y}) \right] \mathrm{d}\Gamma, \tag{15}$$

where $G(\boldsymbol{x},\boldsymbol{y})$ denotes the Green's function satisfying Eq. (2) and whose 3D form is given as

$$G(\boldsymbol{x},\boldsymbol{y}) = \frac{e^{ik|\boldsymbol{x}-\boldsymbol{y}|}}{4\pi|\boldsymbol{x}-\boldsymbol{y}|}. \tag{16}$$

Assuming a thin boundary surface (i.e. $\Gamma \approx \Gamma^+ \approx \Gamma^-$), the associated boundary conditions of the Helmholtz equation can be reformulated using Eqs. 13,14 as follows

$$\mu(\boldsymbol{y}) = 0, p(\boldsymbol{y}) = \overline{p}(\boldsymbol{y}), \quad \text{on} \quad \Gamma_p, \tag{17}$$

$$\sigma(\boldsymbol{y}) = 0, \frac{\partial p(\boldsymbol{y})}{\partial n} = -j\rho_0\omega\overline{v}_n(\boldsymbol{y}), \quad \text{on} \quad \Gamma_v, \tag{18}$$

$$\sigma(\boldsymbol{y}) = -jk\beta\mu(\boldsymbol{y}), \frac{\partial p(\boldsymbol{y})}{\partial n} = -jk\beta p(\boldsymbol{y}), \quad \text{on} \quad \Gamma_Z, \tag{19}$$

where the normalized boundary admittance is defined as $\beta = Z_0/Z_s$. $Z_0 = \rho_0 c$ is the characteristic impedance of the fluid with density ρ_0 and Z_s is the acoustic impedance of the boundary surface. $\overline{p}$ is the prescribed pressure and $\overline{v}_n$ is the prescribed normal velocity. Γ_p, Γ_v, and Γ_Z represent the Dirichlet, Newmann and Robin boundaries, respectively. At each position on the boundary surface, there exists only one independent variable which is either the single- or the double-layer potential. Therefore, the indirect boundary integral formulation Eq. (15) can be reformulated as

$$\begin{aligned} p(\boldsymbol{x}) = &\int_{\Gamma_p} \sigma(\boldsymbol{y})G(\boldsymbol{x},\boldsymbol{y})\mathrm{d}\Gamma_p - \int_{\Gamma_v} \mu(\boldsymbol{y})\frac{\partial G(\boldsymbol{x},\boldsymbol{y})}{\partial n_y}\mathrm{d}\Gamma_v \\ &- \int_{\Gamma_Z} \mu(\boldsymbol{y})\left[\frac{\partial G(\boldsymbol{x},\boldsymbol{y})}{\partial n_y} + jk\beta G(\boldsymbol{x},\boldsymbol{y})\right]\mathrm{d}\Gamma_Z. \end{aligned} \tag{20}$$

Subsequently, Eq. (20) can be used to rewrite the boundary conditions in Eqs. (17)–(19) in a compact form by using a function f of unknowns σ and μ, as follows

$$f_p(\sigma,\mu) = \overline{p}, \quad \text{on} \quad \Gamma_p, \tag{21}$$

$$f_v(\sigma,\mu) = -j\rho_0\omega\overline{v}_n, \quad \text{on} \quad \Gamma_v, \tag{22}$$

$$f_Z(\sigma,\mu) = 0, \quad \text{on} \quad \Gamma_Z. \tag{23}$$

A variational approach is adopted to avoid Hadamard finite-part integrals. The equivalent variational statement of Eqs. (21)–(23) can be written with test functions $\delta\sigma$ and $\delta\mu$ which are typically chosen to be the same as the shape functions:

$$\begin{aligned} &\int_{\Gamma_p} f_p(\sigma,\mu)\delta\sigma\mathrm{d}\Gamma_p + \int_{\Gamma_v} f_v(\sigma,\mu)\delta\mu\mathrm{d}\Gamma_v + \int_{\Gamma_Z} f_Z(\sigma,\mu)\delta\mu\mathrm{d}\Gamma_Z \\ &= \int_{\Gamma_p} \overline{p}\delta\sigma\mathrm{d}\Gamma_p - \int_{\Gamma_v} j\rho_0\omega\overline{v}_n\delta\mu\mathrm{d}\Gamma_v. \end{aligned} \tag{24}$$

The application of conventional BEM in room acoustics is however limited in practice due to its excessive computational requirements for large models and/or at high frequencies. As one of the most efficient acceleration approaches to the conventional BEM, the fast multipole method [12] separates the BEM system into near field assembly and far field approximations based on the relative distances of the boundary variables. The near field pairs, which typically become a small portion of the problem, are directly evaluated via Eq. (24), while the far field pairs can be accelerated via the fast multipole expansions [12]. In this way, the system matrix is not necessarily formulated explicitly, which significantly reduces the memory footprint. Iterative solvers such as generalized minimal residual method (GMRES) can be employed to solve the system efficiently. Together with parallelization implemented, the fast multipole method enables BEM to solve very large acoustic problems in a more efficient way [20].

2.2. Boundary conditions

In room acoustics, the random-incidence (or statistical) absorption coefficient is a quantity describing the energy absorbed by a material with respect to the incident energy. Unlike GA methods, which often deal with the absorption coefficient as the boundary definition, the wave-based methods require a phased representation of the boundary using either a complex surface impedance or a pressure reflection coefficient. However, for most of the commonly used materials in room acoustics, these phased representations are not available [23]. Several methods have been proposed to retrieve the surface impedance from the statistical absorption coefficient [24,25]. It should be noted that this procedure often yields non-unique solutions unless some constraints for the model parameters are available. Nevertheless, research on a more accurate conversion is out of the scope of this paper. Instead, our focus is on the determination of an equivalent boundary definition between a frequency-domain FMBEM and a time-domain FDTD solver.

In the present work, Robin boundary conditions are considered, which benefit from both simplicity and flexibility as they apply to the surface impedance of the boundary. In the FMBEM implementation, the random-incidence sound absorption coefficient can be expressed as a function of the surface impedance as (Ref. [26])

$$\alpha_{\text{random}} = \int_0^{\pi/2} \left(1 - \frac{(Z\cos\phi - 1)^2}{(Z\cos\phi + 1)^2}\right) \sin 2\phi \mathrm{d}\phi, \tag{25}$$

where $Z = Z_s/Z_0$ and ϕ is the incidence angle of the acoustic wave. From Eq. (25), the impedance Z_s can be retrieved using the bisection root-finding method. Fig. 1 shows an example of the estimated Z_s from such a root-finding method.

On the other hand, the employed FDTD solver converts the random-incidence absorption coefficient into a normal-incidence absorption coefficient. Therefore, the acoustic impedance of the surface material Z_s from the FMBEM solver is translated into an input reflection coefficient R for the FDTD solver using

$$R = \frac{Z_s - Z_0}{Z_s + Z_0}. \tag{26}$$

It is also worth mentioning that room surface boundaries are modelled as locally reacting (i.e. the vibration of the boundary caused by the waves in the propagation domain are neglected) in both solvers.

2.3. Acoustic source definition

For simplicity, an omnidirectional sound source is considered in the present work. Due to the nature of the two solvers, the acoustic source is defined and modelled differently in the two schemes.

In the frequency domain, such a source is considered as a frequency-based monopole generating an incident sound field which can be expressed as

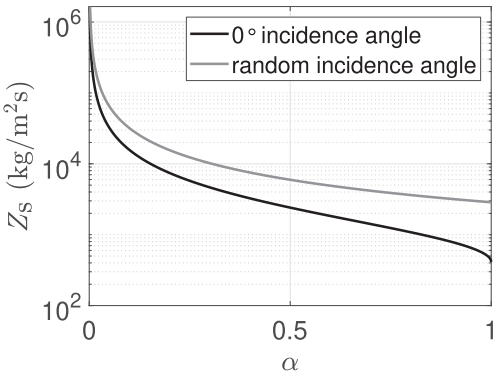

Fig. 1. Surface impedance Z_s as a function of absorption coefficient α for different incidence angles.

$$p_{\text{inc}} = \widehat{S}\frac{e^{-ikd}}{d}, \tag{27}$$

where $\widehat{S}$ is the amplitude of the monopole source and d is the distance from the source.

In time-domain wave-based approaches including the FDTD method, an omnidirectional sound source can be defined in general as a source driving function added at the right-hand side of the wave equation Eq. (3). A commonly used source driving function consists of a discrete delta sequence that is injected at a single grid point in the simulation domain. Such an impulse signal is practical as it is the shortest, thus the most efficient in reducing the overall simulation run-time [27], and since it comprises all frequencies in equal amount.

Another consideration regarding source modeling in FDTD concerns the formulation of the update equation at the source grid point. Different strategies lead to different source types: *hard*, *soft*, and *transparent* source. The *hard* source excitation has the simplest implementation, but introduces a discontinuity in the simulated acoustic field resulting in a shift of resonant modes from expected values [27]. Both the *soft* and *transparent* source implementations avoid the scattering from the source node. However, the *transparent* source excitation requires a pre-calculation of the grid impulse response, which can be impractical for some applications [28]. A *soft* source is chosen here and the source driving function is scaled by $1/X^3$, where X is the spatial grid spacing, to ensure consistency of the source amplitude across different spatial grid spacings [29].

2.4. Time–frequency domain conversion

While the FDTD method is formulated in the time domain and computes the acoustic unknowns with elapsed time, FMBEM solves the time-harmonic acoustic problem in the frequency domain, meaning that the solution is a steady state result at each frequency. In order to evaluate the obtained results from the two solvers, a discrete Fourier transform (DFT) and an inverse DFT (IDFT) are applied as a post-processing step for the time–frequency domain conversion. The DFT of a N-long sequence x_n, which can typically be applied on an FDTD-simulated impulse response, is given as (Ref. [30])

$$X_k = \sum_{n=0}^{N-1} x_n e^{-i\frac{2\pi}{N}kn}. \tag{28}$$

The length of the FDTD simulated impulse response $T = (N-1)/f_s$ (where f_s is the sampling frequency of the time-domain signal) is selected such that sufficient energy decay is observed in the signal to calculate the reverberation time. This also ensures an accurate frequency series after the DFT transformation. Conversely, the IDFT of the N-long sequence X_k is given as (Ref. [30])

$$x_n = \frac{1}{N}\sum_{k=0}^{N-1} X_k e^{i\frac{2\pi}{N}kn}. \tag{29}$$

To ensure a stable conversion, the frequency resolution $\Delta f \leqslant 1/T$ of the FMBEM simulations is defined based on the problem at hand. The determination of the length T of the time-domain signal can be based on either the former FDTD simulation or an estimation of the target reverberation time. It is worth mentioning that the frequency resolution should also be sufficiently fine to ensure that the phase can be unwrapped correctly. In addition, it is necessary to run the frequency domain calculations beyond the crossover frequency (the transition frequency between two, e.g., one-third octave bands or octave bands) to avoid artifacts from the abrupt drop on the frequency response. Ref. [9] suggests to include at least half an octave data points above the crossover frequency. This may not be sufficient if octave-band filters are applied. In such cases, Ref. [31] suggests one extra full octave band. The accuracy of those extra frequency bins are less demanding as they will be heavily attenuated by the crossover filter. As such, a less strict tolerance (e.g., 10^{-2}) can be used for the iterative solver in FMBEM to improve the computational efficiency.

3. Model uncertainties

The quantification of uncertainties is recommended in measurements to assess the reliability of the obtained results [32,33]. Computer-aided room acoustic simulations also induce uncertainties, which indicate the reliability of the model and simulation results. In Ref. [7], uncertainties from GA methods are presented and discussed. The following paragraphs present an overview of the uncertainties when using wave-based methods such as FMBEM and FDTD in room acoustic simulations. The sources of simulation uncertainties typically come from three aspects: the geometrical model of the room, the input of material properties, and the algorithm details of the chosen solver.

3.1. Model geometry

The fidelity of a computer-aided design (CAD) model, e.g., the level of detail (LOD) that should be included in the geometrical model, has a significant impact on the simulation results [34,18]. However, an appropriate LOD is sometimes difficult to identify *a priori*. This often relates to the frequency band of interest and can be case dependent. A convergence study with different levels of detail would help to determine the final LOD.

Furthermore, any given CAD model needs to be discretized to be used in the wave-based numerical solvers. The wave-based methods require an element-based representation of the domain, which normally allows to capture some of the details in the model. Compared to flat surfaces, curved surfaces are generally more challenging for an accurate discretization. This is especially true for the conventional FDTD method which operates over regular grids, thus leading to a staircase approximation of the continuous geometry. If needed, higher accuracy can be achieved by techniques such as the contour path modelling [35] and fitted boundary cells [36]. In BEM/FMBEM, a refined mesh is commonly used for a more accurate modelling of curved surfaces. In addition, the use of high-order curved elements [37] or CAD representation [38] directly may improve the discretization accuracy of the curved surfaces. However, to the best of the authors' knowledge, such advanced modelling techniques have not been applied yet to room acoustic simulations.

3.2. Material data

In room acoustic simulations, defining the correct material properties is a well-known challenge [7,39]. A conventional way is to conduct in situ measurements for the materials in the space. However, the acoustic properties of non-flat surfaces or volumetric objects (e.g., furniture) can be difficult to measure in a straightforward manner. Besides, the available material data from the literature or databases cannot be directly applied to the computer model due to the deviations of the data and incomplete information (e.g., standard deviation of the measurement). In practice, a common approach is to adjust the data until a match with some reference value (e.g., acoustical parameter derived from measured room impulse responses (RIRs) as in Ref. [40]) is attained. However, there is still a question on the reliability of such approaches. Therefore, Section 5 presents an uncertainty sensitivity study on such two sets of absorption coefficients provided in the Benchmark for Room Acoustical Simulation (BRAS) database [39].

3.3. Numerical aspects

The wave-based approaches such as FMBEM and FDTD generate deterministic solutions, which inherently eliminates the stochastic uncertainties from, e.g., the ray tracing method [7]. On the other hand, other numerical errors and uncertainties are present in the wave-based methods. The kernel-related errors create undesired nonphysical effects. For example, the numerical dispersion in FDTD causes a cumulative phase error in wave propagation velocity [17]. In BEM/FMBEM, the solution is known to be polluted by the fictitious frequency from an interior domain [22]. This type of numerical errors are typically well-studied in the literature. Another non-kernel-related uncertainty concerns the solver setup, e.g., discretization of the domain, selection of the acoustic source, convergence, etc. Because the decisions on these options depend on the problem at hand, they can sometimes be difficult to select *a priori*. The convergence of the solver is critical among all the settings as it affects both accuracy and efficiency of the solver. In FMBEM, the convergence concerns the selection of an appropriate tolerance for the iterative solver when a good preconditioner is being used. In FDTD, the selection of temporal sampling frequency is of importance as it directly relates to the degree of numerical dispersion and thus to the accuracy of the simulation results. In the following numerical experiments, the effects and decision of the convergence tolerance in FMBEM and temporal sampling frequency in FDTD are discussed.

4. Numerical experiments

4.1. Numerical setup

Unless otherwise stated, the numerical examples presented in the following sections use a speed of sound value of $c = 343.21$ m/s, corresponding to a propagation speed in dry air at 20 °C. The density of dry air ρ_0 at 20 °C is 1.2041 kg/m^3. An open source FDTD solver [19] was employed to run the FDTD simulations with the SRL scheme. The Courant number λ was set to $1/\sqrt{3}$ which corresponds to the stability limit of the SRL scheme. A *soft* source with a discrete delta function as the driving function was utilized to excite the FDTD grid. To compensate for the accumulation of DC caused by the *soft* source, a DC blocking filter (taken from Ref. [41]) was applied in a post-processing stage to all FDTD simulation results. The FMBEM solver is an in–house implementation using an optimized linear algebra package (LAPACK) routine. Specific to the FMBEM simulations, linear triangular mesh was employed for the discretization of the boundary surfaces. A discretization of at least six elements per wavelength was ensured for the frequency band of interest. Double precision for floating-point numbers was employed for both solvers.

4.2. Convergence tolerance for FMBEM

For large room acoustic simulations, the model size is often out of the range for direct solvers in a conventional BEM due to the extensive memory cost. Utilizing the low rank properties of the matrix, the FMBEM is typically solved by iterative solvers. Such solvers recursively approximate the solution towards the exact solution via an iterative procedure. The iterative solvers based on Krylov subspace, such as GMRES, are commonly used in FMBEM. If a sufficient number of iterations (e.g., up to the number of unknowns) is allowed, the GMRES solver should converge to the exact solution. However, this is typically infeasible in practice as more iterations will cost extensive computational time and memory. Thus, it is of importance to determine an appropriate stopping criterion for the GMRES solver in order to compromise between efficiency and accuracy.

Another important aspect lies in the convergence rate, e.g., the number of iterations to reach the target stopping criterion. For an ill-conditioned system, the GMRES solver may stagnate and struggle to converge [42]. The construction of efficient preconditioner to the system is an active research field. In this discussion, the sparse approximate inverse preconditioner based on Frobenius norm minimization [43] is implemented to improve the convergence.

In the context of room acoustics, a similar convergence study has been presented in Ref. [13] in which the tolerances were chosen as $10^{-1}, 10^{-2}, 10^{-4}$ and 10^{-6} in the discussion. However, the tolerance of 10^{-3} was missing from the study. Besides, the correlation between the selected tolerance and phase angle was not revealed in the discussion. In the following numerical experiment, a cuboid room of size 2 m × 1 m × 1 m is considered. The acoustic source is placed at $[0.04, 0.02, 0.02]$ m. Four receivers are located in the diagonal dimensions of the room as shown in the left schema of Fig. 2. Four tolerances are considered, $\epsilon = [10^{-2}, 10^{-3}, 10^{-4}, 10^{-6}]$, respectively. A uniform frequency-independent absorptive material is defined on the boundary with a constant absorption coefficient of 0.2. The relative differences of complex valued results are computed separately for magnitude and phase by L_2-norm $e_2^p = \|p - p_0\|_2 / \|p_0\|_2$ and $e_2^\theta = \|\theta - \theta_0\|_2 / \|\theta_{ref}\|_2$, where the differences are normalized by the reference magnitude p_0 and reference angle $\theta_{ref} = 2\pi$ respectively [44]. The result of $\epsilon = 10^{-6}$ is used as reference for computing the relative differences.

Fig. 3 shows the relative differences on the magnitude and phase at various receiver locations. The tolerance of $\epsilon = 10^{-2}$ gives the highest deviations in both magnitude and phase in all cases, whereas both $\epsilon = 10^{-3}$ and $\epsilon = 10^{-4}$ show satisfactory accuracy at most of the frequencies if considering a general engineering accuracy of 1%. The result of $\epsilon = 10^{-2}$ in the present case differs from the findings from Ref. [13] in which $\epsilon = 10^{-2}$ is considered to be a sufficient tolerance in a cubic geometry. In the present model configuration, $\epsilon = 10^{-2}$ could not provide adequate accuracy at the receivers. This is due to the fact that the predefined tolerance is maintained on the solution vector of the system. The accuracy of the results at field points can vary to some degree as shown in Fig. 3. It is also observed that the phase difference is generally smaller than the magnitude difference and may demonstrate a different pattern. In addition, it is not surprising that smaller tolerances lead to excessive calculation time, while larger tolerances terminate the simulation early. For instance, at the simulation of 780 Hz, the GMRES solver requires 70, 99, 126, 671 iterations to reach the tolerance of $10^{-2}, 10^{-3}, 10^{-4}, 10^{-5}$, respectively. The

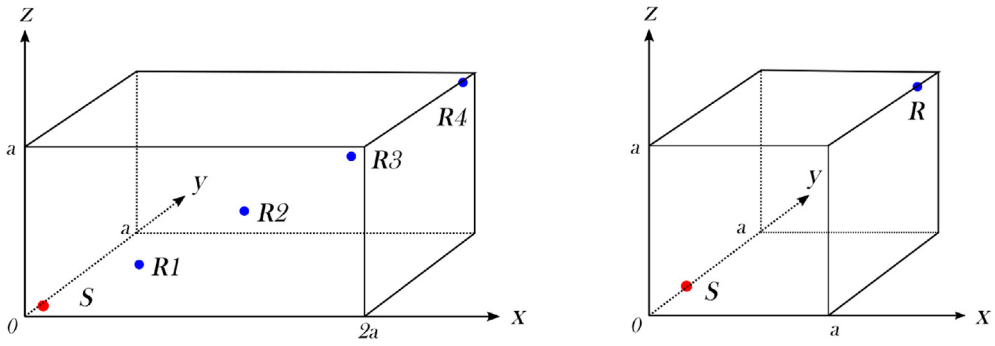

Fig. 2. Models for the numerical experiments: cuboid room (left) and cubic room (right). $a = 1$ m.

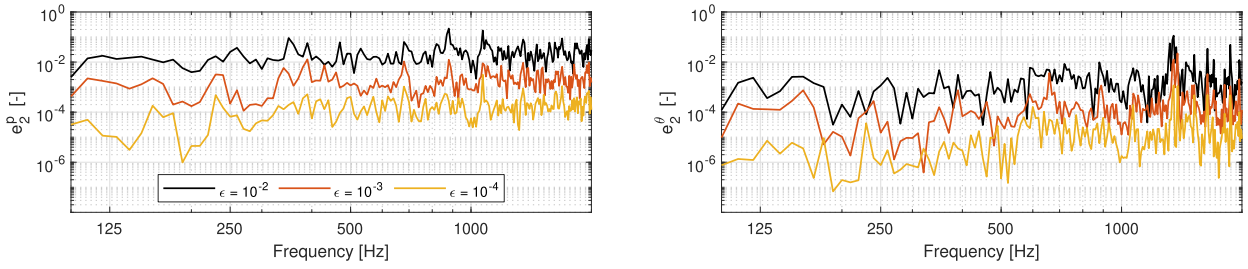

(a) Receiver $R1 = [0.4, 0.2, 0.2]$ m

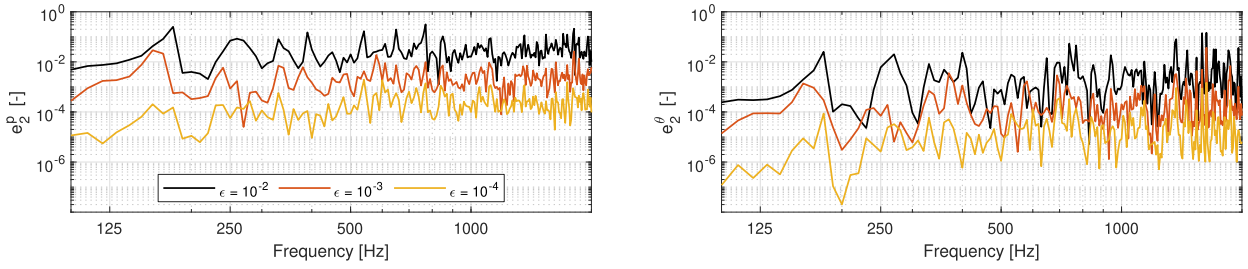

(b) Receiver $R2 = [0.8, 0.4, 0.4]$ m

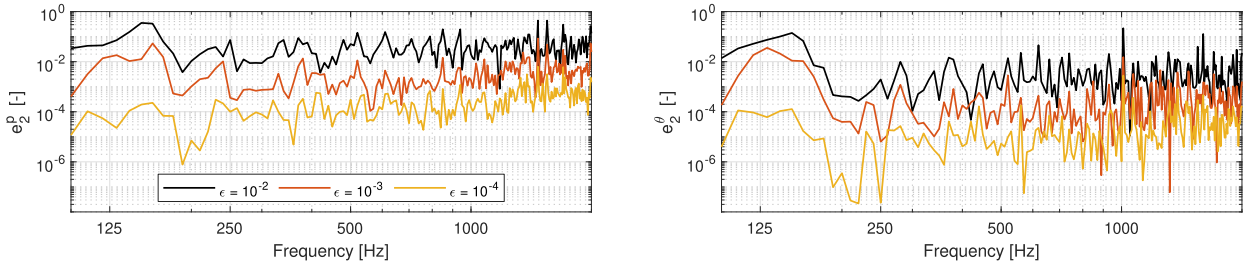

(c) Receiver $R3 = [1.4, 0.7, 0.7]$ m

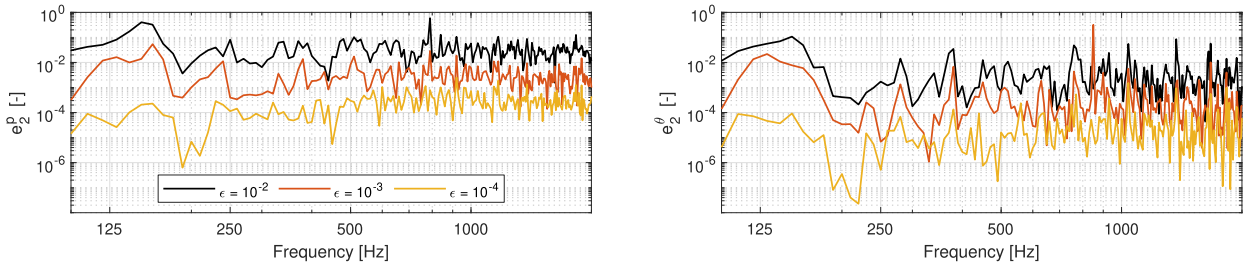

(d) Receiver $R4 = [1.9, 0.95, 0.95]$ m

Fig. 3. Relative differences on the acoustic magnitude (left) and phase (right) for different tolerance settings at various receiver positions. The result of $\epsilon = 10^{-6}$ is used as reference.

selection of $\epsilon = 10^{-3}$ over other finer tolerance, e.g., $\epsilon = 10^{-5}$ can give significant speedup on the iterative solving. It should be mentioned that the condition of the BEM system may vary significantly across bands due to its high dependence on frequency. Thus the convergence behaviour of the solution could also vary accordingly. Depending on the practical application, the choice of an appropriate tolerance can be decided based on the problem at hand. In this analysis, the tolerance of $\epsilon = 10^{-3}$ is a suitable compromise between efficiency and accuracy. A good agreement can be found between the results from FDTD and FMBEM using the tolerance of $\epsilon = 10^{-3}$ in Fig. 4. For very complex scenarios, a smaller ϵ may be needed.

4.3. Temporal sampling frequency for FDTD

Numerical dispersion, also referred to as discretization or dispersion error, is a numerical error inherently present in FDTD simulations. This error is due to the approximation of continuous differential operators by discrete operators and depends on both the propagation direction and the frequency of the simulated sound waves. The extent of numerical dispersion is commonly expressed in a single quantity, that is the relative phase velocity or the percentage of phase velocity error, denoted v_p. Based on this single quantity, an accuracy criterion was defined in Ref. [45] as the frequency band in which the maximum relative numerical error does not exceed 2%. For example, under this definition, the SRL scheme is considered valid up to $0.076 \times f_s$ Hz, where f_s denotes the temporal sampling frequency of the simulation. Based on the same quantity, another accuracy criterion was determined in Ref. [16] using a 10% error limit, leading to a frequency bandwidth valid up to $0.151 \times f_s$ Hz. However, such rules for determining an acceptable error percentage limit cannot be generalized to all possible simulated scenarios. Thus investigating the effect of changing the sampling frequency on the accuracy of the simulation results is of relevance.

Here, such an investigation is conducted on a 1 m × 1 m × 1 m room as shown in the right schema of Fig. 2. Both rigid and absorptive boundaries (with 0.2 absorption coefficient) are considered. The room was simulated for a single source-receiver combination using both FMBEM and FDTD solvers. The source was located at [0.2, 0.2, 0.2] m and the receiver at [0.9, 0.9, 0.9] m. The upper limit of the frequency range of interest was set to f_l = 800 Hz. For each room, the FDTD solver was run separately for one second with three different sampling frequencies. Two out of three sampling frequencies were chosen based on percentages of relative phase velocity at f_l used in other studies: 2% (e.g., as in Refs. [46,45]) and 10% (e.g., as in Ref. [16]), leading to f_s = 800/0.076 = 10526 Hz and f_s = 800/0.151 = 5298 Hz, respectively. The third and highest sampling frequency considered was set to f_s = 800/0.0067 = 119166 Hz, which corresponds to approximately 0.02% of relative phase velocity at f_l. This sampling frequency was chosen such that the spatial grid spacing was fine and close to a fraction of the room dimensions in order to represent the geometry as closely as possible. To provide a reference for the comparison, the analytic eigenfrequencies f_{n_x,n_y,n_z} of the room were also evaluated using (see e.g., Ref. [26])

$$f_{n_x,n_y,n_z} = \frac{c}{2}\sqrt{\left(\frac{n_x}{L_x}\right)^2 + \left(\frac{n_y}{L_y}\right)^2 + \left(\frac{n_z}{L_z}\right)^2}, \tag{30}$$

where L_x, L_y, and L_z are the dimensions of the room (in m). n_x, n_y, and n_z denote the numbers of nodal planes perpendicular to the x-axis, the y-axis and the z- axis, respectively.

The FDTD-simulated pressure responses were Fourier-transformed using Eq. (28) to obtain the magnitude responses shown in Fig. 5. In general, a good agreement between the FMBEM and the analytical solution can be observed. It also can be seen from Fig. 5 that the resonance frequencies simulated using the FDTD method with f_s = 10526 Hz and f_s = 5298 Hz are strongly shifted in comparison to the FMBEM simulation. The shift is observed to a much lower extent when using f_s = 119166 Hz. Besides, the direction of the shift with respect to the analytic eigenfrequencies is towards lower frequencies. This observation is in line with the profile of the phase velocity error indicating that higher frequencies travel at lower speed than lower frequencies. Furthermore, some of the eigenfrequencies simulated using the 10% error limit are missing. These results also indicate that out of

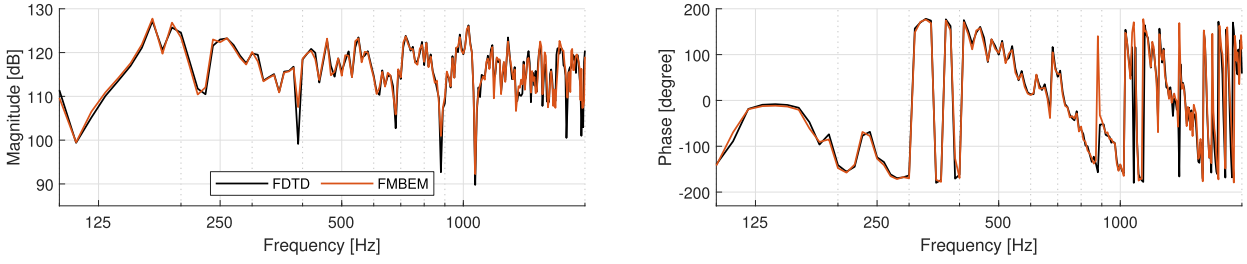

(a) Receiver $R1 = [0.4, 0.2, 0.2]$ m

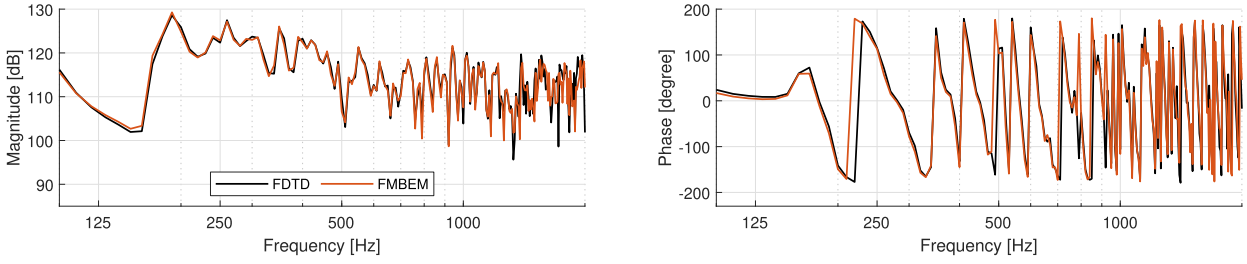

(b) Receiver $R4 = [1.9, 0.95, 0.95]$ m

Fig. 4. Magnitude (left) and phase (right) comparisons of FDTD and FMBEM ($\epsilon = 10^{-3}$) on the cuboid room model at two receivers. The other two receivers gave similar results which are omitted here.

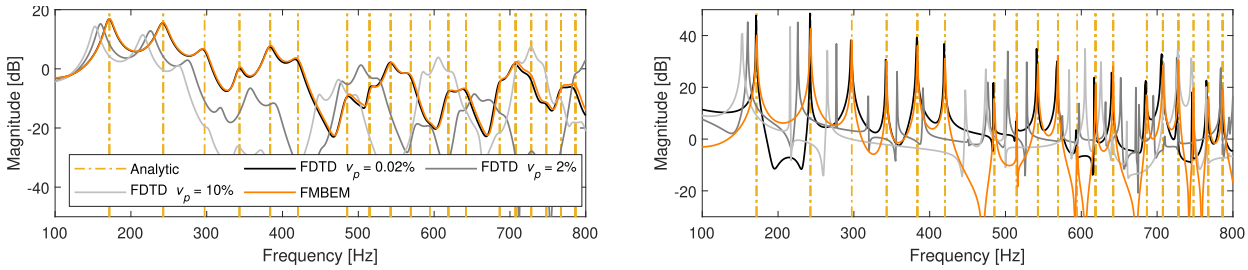

Fig. 5. Magnitude response of the cubic room simulated with FMBEM and FDTD with absorptive boundary condition (left) and rigid boundary condition (right). The FDTD solver was run with the forward difference boundary formulation (see Section 2.1.1).

the three sampling frequencies, only f_s = 119166 Hz is in good agreement with the FMBEM simulation results and the analytic eigenfrequencies. Based on these results, f_s = 119166 Hz was chosen to simulate the room acoustic scenarios presented in Section 5.

5. Room acoustic scenarios

5.1. Scenarios description

In order to evaluate the capability of the two wave-based solvers in simulating scenarios with different complexities, five cases with gradually complexified material input data are considered. All scenarios consisted of the same CAD model corresponding to a small seminar room (volume ≈ 145 m^3) taken from BRAS [39]. BRAS has provided the 3D geometrical model of the room (a perspective view is shown in Fig. 6) and the distribution of five room surface materials: floor, ceiling, concrete, window and plaster. For each material, two different sets of random-incidence absorption coefficients given in 31 third octave bands were provided: i) values based on database values and in situ measurements, which will be hereafter referred to as *initial* absorption coefficients; ii) values adjusted according to Eyring's equation to match the measured reverberation time of the room, which will be hereafter referred to as *fitted* absorption coefficients. The rationale behind the choice of using BRAS was to provide material input data for which a comparison between simulations and measurements was possible. All scenarios included a single source and five receivers whose positions corresponded to measurement positions of RIRs provided in BRAS.

The following list describes the material input data for each simulation scenario:

(a) a single frequency-independent material, whose absorption coefficient is obtained by a linear average of the first 15 bands of the "window" material from the *initial* absorption coefficients
(b) five frequency-independent materials, whose absorption coefficients are obtained by a linear average of the first 15 bands of the corresponding materials from the *initial* absorption coefficients
(c) a single frequency-dependent material, whose absorption coefficients correspond to those of the "window" material from the *initial* absorption coefficients
(d) five frequency-dependent materials, whose absorption coefficients are defined by the corresponding materials from the *initial* absorption coefficients
(e) five frequency-dependent materials, whose absorption coefficients are defined by the corresponding materials from the *fitted* absorption coefficients.

For the FMBEM simulations, a frequency resolution of 0.5 Hz was used for each scenario, which provided a 2-s long impulse response after IDFT. To align with FMBEM, the simulation time of the FDTD solver was 2 s for each scenario.

5.2. Results and discussion

Fig. 7 shows direct comparisons between the FDTD- and FMBEM-simulated magnitude and phase responses for a single receiver position (R1) with different combinations of material input data. The results for the other four receiver positions, which are omitted here for brevity, gave similar comparisons. Applying Eq. (29) to the frequency-domain responses from Fig. 7, the time-domain RIRs were obtained. From these RIRs, the reverberation time (T_{20}), early decay time (*EDT*), clarity (C_{80}), and definition (D_{50}) were evaluated in three octave bands using the function *ita_roomacoustics* from the ITA Matlab Toolbox [47]. The calculated room acoustic parameters are reported in Table 1. The

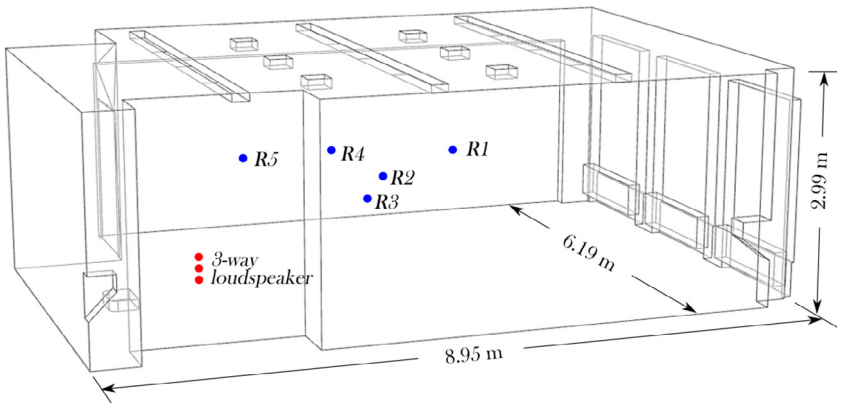

Fig. 6. Perspective view of the 3D geometrical model of the small seminar room (CR2 scene from BRAS). Receiver positions are indicated by the letter "R".

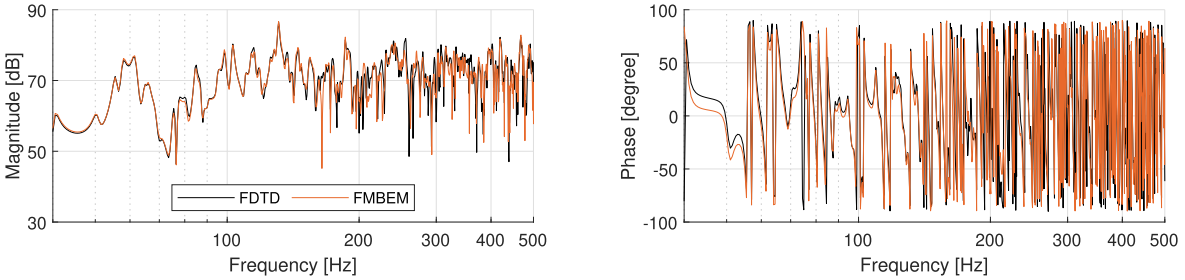

(a) Single frequency-independent material

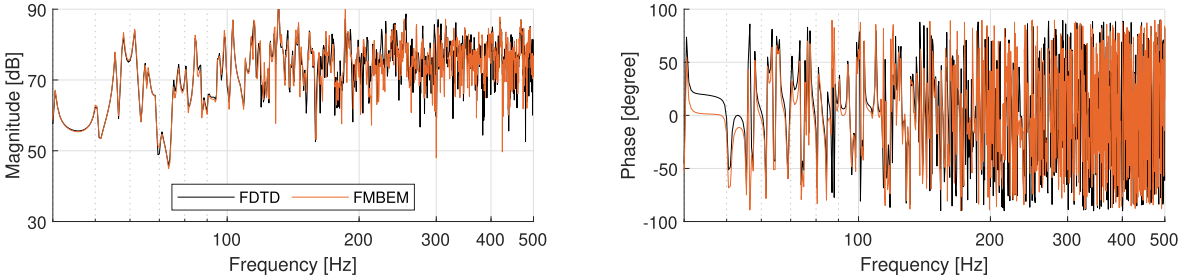

(b) Five frequency-independent materials

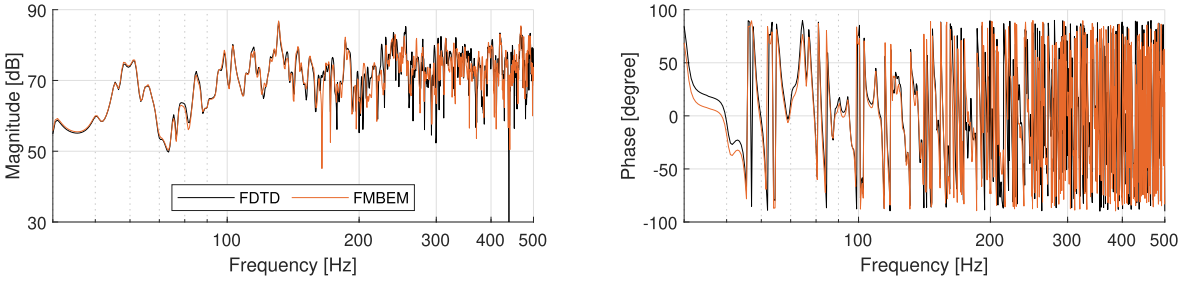

(c) Single frequency-dependent material

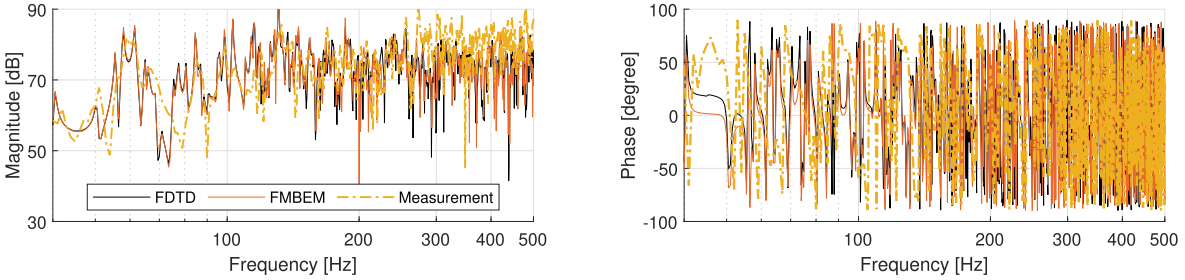

(d) Five frequency-dependent materials (*initial* absorption coefficients)

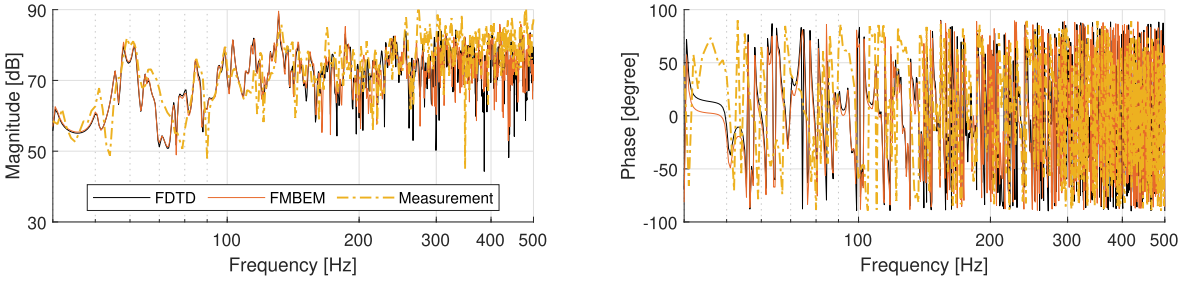

(e) Five frequency-dependent materials (*fitted* absorption coefficients)

Fig. 7. Magnitude (left) and phase (right) responses at the receiver R1 from FDTD and FMBEM simulations with different material input data complexity.

recommended just noticeable difference (JND) values for each parameter are given by Ref. [48]. These values are considered as good indicators for the comparison of the two solvers.

As shown in Fig. 7a, a good agreement is obtained for case (a), where a single absorption coefficient is assigned to all room surfaces. This case has a similar setup compared to the cubic and cuboid rooms discussed in Sections 4.3 and 4.2, whereas the geometrical complexity differs significantly. For the same complex geometry, both FMBEM and FDTD can provide very close acoustic predictions over a wide frequency band, although small deviations are observed as the frequency increases. This indicates that both solvers can capture the characteristics of the CAD model. Similar findings can be observed by examining the predicted room acoustic parameters, where the difference between the two solvers is maintained below the JND for most of the entries. A slightly higher difference between the two solvers is found for EDT at 250 Hz.

In case (b), all five materials with frequency-independent absorption coefficients in the room are considered. A good match has been maintained in the low frequency band as shown in Fig. 7b. Similarly to case (a), small deviations appear at higher frequencies, leading to a slightly higher deviation for the T_{20} and *EDT* at 125 Hz. For the other entries in Table 1, the difference between the predictions of the two solvers is maintained under JND. These results suggest that both solvers are capable of handling various frequency-independent materials. The differences observed are perhaps due to the accumulated errors from the reflections of the acoustic waves at different boundary conditions.

Case (c) takes a single frequency-dependent material in the room. The simulation of the FMBEM is straightforward in this case as it inherently solves the problem per input frequency. Since the employed FDTD solver does not handle frequency-dependent boundary conditions, a series of FDTD simulations are run for all one-third octave bands which correspond to the available absorption coefficients from BRAS. Twelve sets of absorption coefficients are provided to cover the bandwidth of interest (40 – 500 Hz), which leads to a total of twelve FDTD simulations. Each simulation output was then Fourier-transformed using Eq. (28). The Fourier transforms were combined in a single frequency-dependent response according to their respective one-third octave band. As the result shown in Fig. 7c, the frequency responses from the two solvers are matching as good as previous cases. For all the room acoustic parameters, the difference between the two solvers is maintained under JND except the *EDT* at 250 Hz, which is a similar to case (a).

The final cases (d) and (e) consider all five frequency-dependent materials in the numerical model, and thus represent scenarios close to reality. As such, the measured RIRs collected from BRAS are also presented as part of the comparison. The two numerical solvers give close predictions in both magnitude and phase responses although some deviations are shown at higher frequencies. For the majority of the room acoustic parameters, the difference between the two solvers is within the JND, whereas the T_{20} (at 250 Hz in case (d) and at 125 Hz in case (e)) and EDT (at 125 Hz) demonstrate slightly higher deviations. This finding is similar to case (b). However, large discrepancies are observed between the simulated and measured results both in room acoustic parameters and frequency responses, as seen in Table 1 and Fig. 7e.

For all the cases, the two solvers can predict convincing results in the lower frequency range, i.e. at 62.5 Hz center frequency. For the parameter C_{80}, both solvers predict values whose difference is within the JND at all bands of interest and for all scenarios. However, it seems that the two solvers predict slightly different T_{20} and *EDT* values at 125 Hz and 250 Hz, especially when multiple materials are included in the room. The definition D_{50}, which describes the early to total sound energy ratio, is also affected. On the other hand, including frequency-dependent materials does not seem to produce larger differences between the results from the two solvers in comparison to frequency-independent materials. This latter observation can be made by comparing case (b) with case (d)-(e) (multiple materials), as well as in the comparison of case (a) and (c) (single material). Since the numerical results are very close to each other, the discrepancies observed with the measurements are likely due to the incorrect material input data. Thus, the following section presents an uncertainty sensitivity study of the *initial* and *fitted* absorption coefficients.

5.3. Uncertainties of material data

To better understand the deviations observed between the results from the simulations and the measurement shown in Fig. 7d–7e and Table 1, uncertainties of the material input data are quantified using the error propagation theory. The error propagation formulation is adapted to the acoustic parameter of interest. Here, the standard deviations of reverberation time are presented based on the formulations from Ref. [7].

Considering Sabine's equation, the reverberation time at 20 °C is given by

Table 1
Room acoustic parameters of the five scenarios (values are averaged over five receivers). Cases for which the difference between the two solvers exceeded the JND are indicated in bold.

		T_{20} (s)			*EDT* (s)			C_{80} (dB)			*D*50 (%)		
Center frequency (Hz)		62.5	125	250	62.5	125	250	62.5	125	250	62.5	125	250
a	FMBEM	1.41	1.46	1.17	1.50	1.51	**1.19**	3.0	1.9	2.6	55.9	44.9	49.1
	FDTD	1.43	1.42	1.24	1.50	1.54	**1.34**	3.0	2.0	2.3	55.6	45.4	47.9
b	FMBEM	3.58	**3.51**	3.01	3.57	**3.69**	3.06	−2.9	−3.9	−3.2	26.9	**19.9**	23.0
	FDTD	3.58	**3.31**	2.92	3.45	**3.26**	3.13	−2.7	−3.5	−3.6	27.7	**21.2**	22.0
c	FMBEM	1.25	1.48	1.66	1.21	1.51	**1.66**	4.4	1.7	0.5	62.7	44.2	39.2
	FDTD	1.25	1.45	1.72	1.21	1.55	**1.86**	4.4	1.9	0.1	62.3	44.7	37.7
d	FMBEM	3.78	3.33	**1.91**	3.95	**3.41**	1.80	−3.4	−3.5	0.2	24.8	**21.6**	37.2
	FDTD	3.71	3.20	**1.74**	3.77	**2.97**	1.87	−3.1	−3.0	0.2	26.0	**23.3**	38.0
e	FMBEM	2.30	**2.03**	1.96	2.11	**1.86**	1.92	0.7	−0.2	−0.3	44.5	35.6	35.1
	FDTD	2.22	**1.88**	1.89	2.06	**1.76**	2.02	1.1	0.3	−0.5	46.2	37.7	35.0
	Measurement	1.74	1.35	1.63	1.54	1.40	1.52	3.9	2.8	1.0	58.0	44.3	40.2
	JND		5%[1]			5%[1]			1 dB[1]			5%[1]	

*According to Ref. [48].

$$T = \frac{0.161V}{S_A}, \tag{31}$$

where V is the volume of the room. $S_A = \sum_i S_i \alpha_i$ where S_i and α_i are the surface area and the absorption coefficient of the i material constituting the room, respectively.

Since the variables α_i are independent from each other, the uncorrelated error propagation into the uncertainty of the equivalent absorption can be derived [7] as

$$\sigma_{S_A}^2 \approx \left(\frac{\partial S_A}{\partial \alpha_1}\sigma_{\alpha_1}\right)^2 + \left(\frac{\partial S_A}{\partial \alpha_2}\sigma_{\alpha_2}\right)^2 + \ldots, \tag{32}$$

which yields

$$\frac{\sigma_{S_A}}{S_A} = \frac{\sqrt{\sum_i (S_i \sigma_{\alpha_i})^2}}{\sum_i S_i \alpha_i} = \frac{\sigma_T}{T} \leqslant JND. \tag{33}$$

The relative standard deviation of $T, \sigma_T/T$, is equal to the relative standard deviation of the equivalent absorption area σ_{S_A}/S_A considering the linear correlation between T and S_A from Eq. (31).

Both the *initial* and *fitted* absorption coefficients are considered in the uncertainty calculations. For different combinations of three-out-of-five arbitrarily chosen input materials, Fig. 8 gives the combined limen of their maximum standard deviations to achieve the JND of reverberation time. For each plot in Fig. 8, the inner volume (from the origin of the coordinates to the limen) represents the uncertainties under JND. The limen of JND for materials is band-dependent. Fig. 8a gives an example of the correlated limen at center frequency of 50 Hz, 200 Hz and a linear average of 15 bands. For brevity, the averaged limen is presented in the rest of the study.

It is observed that different materials yield different ranges of standard deviations of the absorption coefficient. For example, the window has shown the largest possible standard deviation, while the ceiling and floor would have limited range for standard deviation. Compared to the *initial* absorption coefficients, the *fitted* absorption coefficients provide a wider range of standard deviations for all the materials. However, the standard deviations from both sets of absorption coefficients yield narrow ranges, of which the maximum is 0.04. This becomes even smaller when considering the correlation among several materials. Nevertheless, these standard deviations are hardly met in real measurements based on ISO 354 [33] and even in impedance tube measurements [49]. With this in consideration, in situ measurement is considered necessary in this case to improve the simulated results in order to match measurements. Besides, the approach of adjusting the input material to match the Eyring's equation does not seem to provide

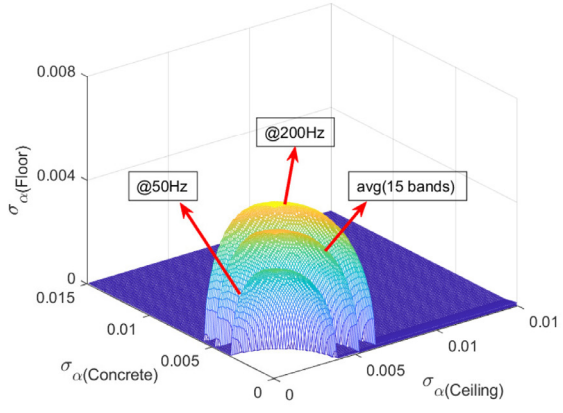

(a) Limen at two one-third octave bands and a linear average of 15 bands (*initial* absorption coefficients).

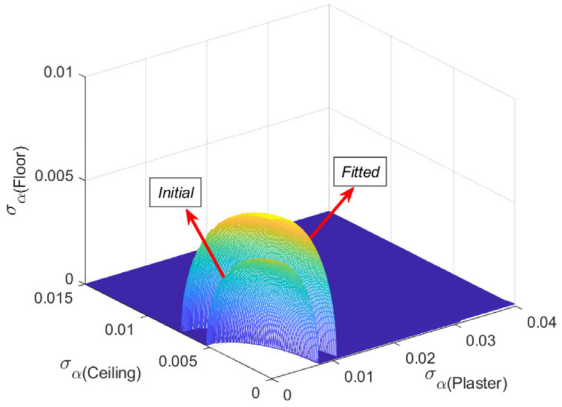

(b) Correlated limen of ceiling, plaster and floor.

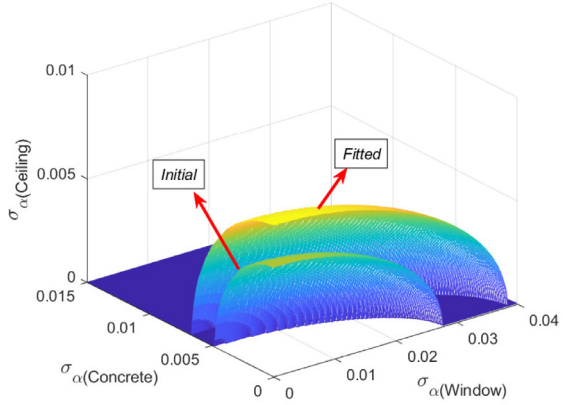

(c) Correlated limen of concrete, window and ceiling.

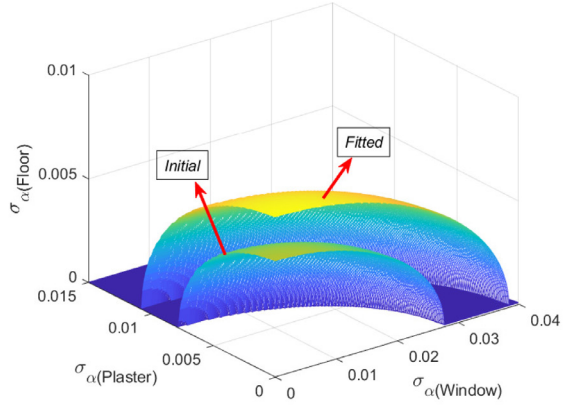

(d) Correlated limen of plaster, window and floor.

Fig. 8. Correlated limen of the maximum standard deviations σ of three random materials to achieve the JND of the reverberation time. (b)-(d) use a linear average of 15 bands of the corresponding absorption coefficients.

convincing material properties. A more reliable way to adjust the material input data can be of interest to investigate in the future. It should also be noted that the boundary conditions in the simulations are modelled as locally reactive, and the acoustic source is simplified as omnidirectional.

5.4. Computational efficiency

Comparing the efficiency of two different solvers in a fair manner is non-trivial as the numerical schemes, architecture, implementation, and parallelization strategies can differ substantially. The numerical complexities of the two solvers are estimated as follows. Consider a 3D problem with size kA, where k is the wavenumber, and A is the characteristic length of the problem. In the FDTD method, the volumetric simulation domain is discretized, which results in $N \sim (kA)^3$ unknowns. The complexity of the explicit FDTD formulation for each time step can be considered as linear [50]. Thus for M time steps, the time complexity of FDTD is $\mathcal{O}\left(M(kA)^3\right)$ and the memory requirement scales with $\mathcal{O}\left((kA)^3\right)$. In FMBEM, the problem is discretized merely on the boundary which gives a number of $N \sim (kA)^2$ unknowns. The computational time and memory requirement of FMBEM are roughly $\mathcal{O}(NlogN)$ when the preconditioner is constructed with a constant number of steps. For M frequencies, the total cost of FMBEM becomes $\mathcal{O}\left(M(kA)^2 log(kA)\right)$.

In the realization of the algorithms, the explicit FDTD scheme is relatively easy to implement and convenient for parallelization, especially using many-core architecture [16,19]. As an example, for a frequency independent boundary definition, running a two second-long FDTD simulation of the small seminar room (volume is 145 m^3, see Section 5) using four GPUs (NVIDIA Tesla P100 with 3584 CUDA cores) in parallel, the total computational time is approximately 3 h using a high sampling frequency f_s = 119166 Hz (corresponding to a cubic cell size of approximately 5 mm). This results in $N \sim 1.2$ billion unknowns and gives results that are considered valid in the full audible frequency range (by using the formula $f_l/f_s = 20000/119166 = 0.196$, where 0.196 is the lowest normalized cutoff frequency of the SRL scheme [17]). By reducing the sampling frequency by two, the number of unknowns is significantly dropped to 150 million, and the computational time reduces to less than 20 min. It is worth mentioning that the Schroeder frequency of this case is estimated to be around 216 Hz using the linear average of the first six octave bands of the measured reverberation time.

In contrast, the FMBEM solver is accelerated by multi-threading on the frequency level. To maximize the solver efficiency, two mesh resolutions are generated according to the target frequencies. For the same room model, the coarse mesh model consisting of 21 thousand unknowns gives a valid frequency range up to 276 Hz, while the fine mesh model consisting of 72 thousand unknowns gives a valid frequency range up to 535 Hz under the rule of six elements per wavelength. For a broadband analysis of 40 – 500 Hz with 0.5 Hz resolution, the total computational time for 921 simulations is approximately 12 h on a desktop with a 10-core CPU (Intel Xeon W-2155 @ 3.3 GHz). As for a comparison, the total computational time for a conventional BEM is estimated to be 161 h (17 min for each coarse mesh simulation and 3.3 h for each fine mesh simulation). The computation times presented above are total wall-clock time excluding the post-processing time.

With the acceleration of parallel computing and modern HPC clusters (typically equipped with a few hundreds of CPU cores and/or several GPUs with thousands of CUDA cores), both solvers are able to simulate sizeable room acoustic problems within a reasonable time in practice.

6. Conclusion

This paper presented a study on two wave-based methods, namely FDTD and FMBEM, in the context of room acoustic modelling and simulations. An overview of the sources of the uncertainty from the two wave-based methods was presented, with the aim of providing guidelines for a reliable control of simulations in large complex scenarios. Numerical experiments were conducted to address the convergence issues of the two solvers, more specifically, the selection of the convergence tolerance in FMBEM and the temporal sampling frequency in FDTD. In order to evaluate the capability of the two solvers in simulating complex scenarios, five material input data-sets with increasing complexity were considered. The simulation results from these five scenarios indicated that the two solvers provide similar predictions for various room acoustic parameters. The predicted room acoustic parameters from the simulations also suggested that considering the frequency dependency of the input materials does not cause additional uncertainty to the results of the two solvers. However, including several materials in the acoustic problem resulted in slightly higher deviations on T_{20} and EDT at higher frequency bands. Besides, large deviations were found between the measurements and the simulation results regardless of the choice of the material input data-set. To explain these deviations, the uncertainty of the two material input data-sets considered for comparing the simulations with the measurements was quantified. This quantification revealed that the material input data-sets yielded large uncertainty on the reverberation time, which implies that such data-sets can hardly represent the actual material properties of the room and that in situ measurements would be required if a higher correlation of simulations and measurements is desired.

7. CRediT authorship contribution statement

Yue Li: Conceptualization, Methodology, Software, Validation, Formal analysis, Investigation, Data curation, Visualization, Writing - original draft & review & editing. **Julie Meyer**: Methodology, Software, Validation, Formal analysis, Investigation, Data curation, Writing - original draft & review & editing. **Tapio Lokki**: Resources, Writing - review & editing. **Jacques Cuenca**: Resources, Writing - review & editing. **Onur Atak**: Resources, Writing - review & editing. **Wim Desmet**: Resources, Writing - review & editing.

CRediT authorship contribution statement

Yue Li: Conceptualization, Methodology, Software, Validation, Formal analysis, Investigation, Data curation, Visualization, Writing - original draft, Writing - review & editing. **Julie Meyer:** Methodology, Software, Validation, Formal analysis, Investigation, Data curation, Writing - original draft, Writing - review & editing. **Tapio Lokki:** Resources, Writing - review & editing, Funding acquisition. **Jacques Cuenca:** Resources, Writing - review & editing, Funding acquisition. **Onur Atak:** Resources, Writing - review & editing, Funding acquisition. **Wim Desmet:** Resources, Writing - review & editing, Funding acquisition.

Declaration of Competing Interest

The authors declare that they have no known competing financial interests or personal relationships that could have appeared to influence the work reported in this paper.

Acknowledgement

This research has received funding from the European Union's Horizon 2020 research and innovation programme under grant agreement No. 721536. Aalto Science-IT project is acknowledged for providing the computational resources necessary to run the FDTD simulations.

References

[1] Pelzer S, Aspöck L, Schröder D, Vorländer M. Integrating real-time room acoustics simulation into a CAD modeling software to enhance the architectural design process. Buildings 2014;4(2):113–38.
[2] M. Vorländer, Acoustic virtual reality systems, in: Auralization, Springer, 2020, pp. 323–331.
[3] Allen JB, Berkley DA. Image method for efficiently simulating small-room acoustics. J Acoust Society Am 1979;65(4):943–50.
[4] Mechel F. Improved mirror source method in roomacoustics. J Sound Vib 2002;256(5):873–940.
[5] Krokstad A, Strom S, Sorsdal S. Calculating the acoustical room response by the use of a ray tracing technique. J Sound Vib 1968;8(1):118–25.
[6] Okada M, Onoye T, Kobayashi W. A ray tracing simulation of sound diffraction based on the analytic secondary source model. IEEE Trans Audio, Speech, Language Processing 2012;20(9):2448–60.
[7] Vorländer M. Computer simulations in room acoustics: Concepts and uncertainties. J Acoust Soc Am 2013;133(3):1203–13.
[8] Brinkmann F, Aspöck L, Ackermann D, Lepa S, Vorländer M, Weinzierl S. A round robin on room acoustical simulation and auralization. J Acoust Soc Am 2019;145(4):2746–60.
[9] Aretz M, Nöthen R, Vorländer M, Schröder D. Combined broadband impulse responses using FEM and hybrid ray-based methods. In: Proceedings of the EAA Symposium on Auralization, Espoo, Finland. p. 15–7.
[10] Thydal T, Pind F, Jeong C-H, Engsig-Karup AP. Experimental validation and uncertainty quantification in wave-based computational room acoustics. Appl Acoust 2021;178:107939.
[11] Kirkup S. The boundary element method in acoustics: A survey. Appl Sci 2019;9(8):1642.
[12] Rokhlin V. Diagonal forms of translation operators for the Helmholtz equation in three dimensions. Appl Comput Harmonic Anal 1993;1(1):82–93.
[13] Yasuda Y, Saito K, Sekine H. Effects of the convergence tolerance of iterative methods used in the boundary element method on the calculation results of sound fields in rooms. Appl Acoust 2020;157:106997.
[14] Gumerov NA, Duraiswami R. Fast multipole accelerated boundary element methods for room acoustics. J Acoust Soc Am 2021;150(3):1707–20.
[15] Marburg S, Schneider S. Performance of iterative solvers for acoustic problems. Part I. Solvers and effect of diagonal preconditioning. Eng Anal Boundary Elem 2003;27(7):727–50.
[16] Savioja L, Real-time 3D finite-difference time-domain simulation of low-and mid-frequency room acoustics, in: Proceedings of the 13th International Conference on Digital Audio Effects, DAFx Graz, Austria, Vol. 1, 2010, p. 75.
[17] Kowalczyk K, Van Walstijn M. Room acoustics simulation using 3-D compact explicit FDTD schemes. IEEE Trans Audio, Speech, Language Processing 2010;19(1):34–46.
[18] Bradley DT, Wang LM. Effect of model detail level on room acoustic computer simulations. J Acoust Soc Am 2002;111(5):2389.
[19] Saarelma J, Savioja L, An open source finite-difference time-domain solver for room acoustics using graphics processing units. In: Forum Acusticum, Krakow, Poland, 2014, p. SS11.8.
[20] Barba LA, Yokota R, Exafmm: An open source library for fast multipole methods aimed towards exascale systems, Boston: Boston University. Retrieved from barbagroup: http://barbagroup. bu. edu (2011).
[21] Bilbao SD, Wave and scattering methods for the numerical integration of partial differential equations, Ph.D. thesis, Stanford University (2001).
[22] Vlahopoulos N, Indirect variational boundary element method in acoustics. In: T. Wu (Ed.), Boundary element acoustics fundamentals and computer codes, WIT Press, 2002, Ch. 6, pp. 83–115.
[23] Lam YW. Issues for computer modelling of room acoustics in non-concert hall settings. Acoust Sci Technol 2005;26(2):145–55.
[24] Jeong C-H. Converting Sabine absorption coefficients to random incidence absorption coefficients. J Acoust Soc Am 2013;133(6):3951–62.
[25] Mondet B, Brunskog J, Jeong C-H, Rindel JH. From absorption to impedance: Enhancing boundary conditions in room acoustic simulations. Appl Acoust 2020;157:106884.
[26] Kuttruff H. Room acoustics. CRC Press; 2016.
[27] Murphy DT, Southern A, Savioja L. Source excitation strategies for obtaining impulse responses in finite difference time domain room acoustics simulation. Appl Acoust 2014;82:6–14.
[28] Sheaffer J, van Walstijn M, Fazenda B. Physical and numerical constraints in source modeling for finite difference simulation of room acoustics. J Acoust Soc Am 2014;135(1):251–61.
[29] Botts J, Savioja L. Effects of sources on time-domain finite difference models. J Acoust Soc Am 2014;136(1):242–7.
[30] Smith S. Digital signal processing: a practical guide for engineers and scientists. Elsevier; 2013.
[31] Hargreaves JA, Rendell LR, Lam YW. A framework for auralization of boundary element method simulations including source and receiver directivity. J Acoust Soc Am 2019;145(4):2625–37.
[32] Joint Committee for Guides in Metrology, Evaluation of measurement data–Guide to the expression of uncertainty in measurement, International Organisation for Standardization (ISO), Geneva, ISBN 50 (2008) 134.
[33] International Organization for Standardization, ISO 354. Acoustics – Measurement of sound absorption in a reverberation room, Geneva (2003).
[34] Pelzer S, Vorländer M, Maempel H-J. Room modeling for acoustic simulation and auralization tasks: Resolution of structural detail. In: Proceedings of the German Annual Conference on Acoustics. Berlin, Germany: DAGA; 2010. p. 15–8.
[35] Jurgens TG, Taflove A, Umashankar K, Moore TG. Finite-difference time-domain modeling of curved surfaces. IEEE Trans Antennas Propag 1992;40 (4):357–66.
[36] Bilbao S. Modeling of complex geometries and boundary conditions in finite difference/finite volume time domain room acoustics simulation. IEEE Trans Audio, Speech, Language Processing 2013;21(7):1524–33.
[37] Ziel V, Bériot H, Atak O, Gabard G. Comparison of 2D boundary curving methods with modal shape functions and a piecewise linear target mesh. Procedia Eng 2017;203:91–101.
[38] Inci EO, Coox L, Atak O, Deckers E, Desmet W. Applications of an isogeometric indirect boundary element method and the importance of accurate geometrical representation in acoustic problems. Eng Anal Boundary Elem 2020;110:124–36.
[39] Brinkmann F, Aspöck L, Ackermann D, Opdam R, Vorländer M, Weinzierl S. A benchmark for room acoustical simulation. concept and database. Appl Acoust 2021;176:107867.
[40] Postma BN, Katz BF. Creation and calibration method of acoustical models for historic virtual reality auralizations. Virtual Reality 2015;19(3–4):161–80.
[41] De Freitas J, The DC Blocking Filter, last accessed: 19-May 2021 (2007). URL: https://se.mathworks.com/matlabcentral/fileexchange/13792-the-dc-blocking-filter.
[42] Zavorin I, O'Leary D, Elman H. Complete stagnation of GMRES. Linear Algebra Appl 2003;367:165–83.
[43] Huckle T. Approximate sparsity patterns for the inverse of a matrix and preconditioning. Appl Numer Math 1999;30(2–3):291–303.
[44] Marburg S. Six boundary elements per wavelength: Is that enough? J Comput Acoust 2002;10(01):25–51.
[45] Kowalczyk K, Van Walstijn M. Room acoustics simulation using 3-D compact explicit FDTD schemes. IEEE Trans Audio, Speech, Language Processing 2011;19(1):34–46.
[46] Saarelma J, Botts J, Hamilton B, Savioja L. Audibility of dispersion error in room acoustic finite-difference time-domain simulation as a function of simulation distance. J Acoust Soc Am 2016;139(4):1822–32.
[47] Dietrich P, Guski M, Pollow M, Masiero B, Müller-Trapet M, Scharrer R, Vorländer M. The ITA-Toolbox: an open source Matlab toolbox for acoustic measurements and signal processing. In: Proceedings of the German Annual Conference on Acoustics, Kiel, Germany. p. 222–5.
[48] International Organization for Standardization, ISO 3382-1. Acoustics - Measurement of room acoustic parameters - Part 1: Performance spaces, Geneva (2009).
[49] Horoshenkov KV, Khan A, Bécot F-X, Jaouen L, Sgard F, Renault A, Amirouche N, Pompoli F, Prodi N, Bonfiglio P, et al. Reproducibility experiments on measuring acoustical properties of rigid-frame porous media (round-robin tests). J Acoust Soc Am 2007;122(1):345–53.
[50] Gaffar M, Jiao D. An explicit and unconditionally stable FDTD method for electromagnetic analysis. IEEE Trans Microw Theory Tech 2014;62 (11):2538–50.